Title

YR36/WKS1-Mediated Phosphorylation of PsbO, an Extrinsic Member of Photosystem II, Inhibits Photosynthesis and Confers Stripe Rust Resistance in Wheat

Journal

Molecular Plant, 12(12)

ISSN

1674-2052

Authors

Wang, Shuai
Li, Qiu-Ping
Wang, Jianfeng
et al.

Publication Date

2019-12-01

DOI

10.1016/j.molp.2019.10.005

Peer reviewed

Journal Pre-proof

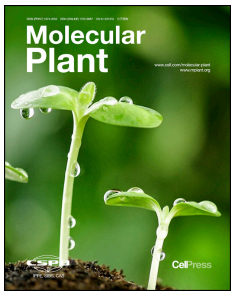

YR36/WKS1-mediated Phosphorylation of PsbO, an Extrinsic Member of Photosystem II, Inhibits Photosynthesis and Confers Stripe Rust Resistance in Wheat

Shuai Wang, Qiu-Ping Li, Jianfeng Wang, Yan Yan, Guo-Liang Zhang, Yan Yan, Huifei Zhang, Jiajie Wu, Feng Chen, Xiaojie Wang, Zhensheng Kang, Jorge Dubcovsky, Jin-Ying Gou

PII: S1674-2052(19)30330-2
DOI: https://doi.org/10.1016/j.molp.2019.10.005
Reference: MOLP 835

To appear in: *MOLECULAR PLANT*
Accepted Date: 7 October 2019

Please cite this article as: **Wang S., Li Q.-P., Wang J., Yan Y., Zhang G.-L., Yan Y., Zhang H., Wu J., Chen F., Wang X., Kang Z., Dubcovsky J., and Gou J.-Y.** (2019). YR36/WKS1-mediated Phosphorylation of PsbO, an Extrinsic Member of Photosystem II, Inhibits Photosynthesis and Confers Stripe Rust Resistance in Wheat. Mol. Plant. doi: https://doi.org/10.1016/j.molp.2019.10.005.

YR36/WKS1-mediated Phosphorylation of PsbO, an Extrinsic Member of Photosystem II, Inhibits Photosynthesis and Confers Stripe Rust Resistance in Wheat

Shuai Wang[1,7], Qiu-Ping Li[1,7], Jianfeng Wang[2], Yan Yan[1,3], Guo-Liang Zhang[1], Yan Yan[1], Huifei Zhang[4], Jiajie Wu[4], Feng Chen[3], Xiaojie Wang[2], Zhensheng Kang[2], Jorge Dubcovsky[5,6] and Jin-Ying Gou[1*]

[1]State Key Laboratory of Genetic Engineering, MOE Engineering Research Center of Gene Technology, Institute of Plant Biology, School of Life Sciences, Fudan University, Shanghai 200438, China

[2]State Key Laboratory of Crop Stress Biology for Arid Areas and College of Plant Protection, Northwest A & F University, Yangling, Shaanxi 712100, China

[3]Agronomy College/National Key Laboratory of Wheat and Maize Crop Science, Henan Agricultural University, Zhengzhou, Henan 450046, China

[4]State Key Laboratory of Crop Biology/College of Agronomy, Shandong Agricultural University, Tai'an, Shandong 271018, China

[5]Department of Plant Sciences, University of California, Davis, California 95616, USA

[6]Howard Hughes Medical Institute, Chevy Chase, Maryland 20815, USA

[7]These authors contribute equally to this work

*Correspondence: jygou@fudan.edu.cn

Running title: WKS1 phosphorylates PsbO to confer *Pst* resistance

Short Summary:

Stripe rust is a devastating disease of wheat, causing significant global grain yield losses. This study shows that WKS1 interacts with and phosphorylates PsbO, an extrinsic member of photosystem II, leads a fast degradation of PsbO by proteases, to reduce photosynthesis and regulate leaf chlorosis in conferring *Pst* resistance. These findings highlight the importance of chlorosis during fungal resistance.

ABSTRACT

Wheat stripe rust, due to infection by *Puccinia striiformis* f. sp. *tritici* (*Pst*), is a devastating disease that is causing significant global grain yield losses. *Yr36*, which encodes the Wheat Kinase START1 (WKS1), is an effective high-temperature adult-plant resistance gene and confers resistance to a broad spectrum of *Pst* races. We previously showed that WKS1 phosphorylates the thylakoid ascorbate peroxidase (tAPX) protein and reduces its ability to detoxify peroxides, which may contribute to the accumulation of reactive oxygen species (ROS). WKS1-mediated *Pst* resistance is accompanied by leaf chlorosis in the *Pst*-infected regions, but the underlying mechanisms remain still elusive. Here, we show that WKS1 interacts with and phosphorylates PsbO, an extrinsic member of photosystem II (PSII), to reduce photosynthesis and regulate leaf chlorosis in conferring *Pst* resistance. A point mutation in *PsbO-A1* or reductions in its transcript levels by RNA interference resulted in chlorosis and reduced Pst sporulation. Biochemical analyses revealed that WKS1 phosphorylates PsbO at two conserved amino acids involved in its physical interactions with PSII and reduces the binding affinity of PsbO to PSII. Phosphorylated PsbO dissociated from the PSII protein complex, and underwent fast degradation by cysteine and aspartic proteases. Taken together, these results demonstrate that perturbations of wheat PsbO by point mutation or its phosphorylation by WKS1 reduce photosynthesis rate and delays the growth of Pst pathogen before the induction of ROS.

Key words: wheat, stripe rust, *Puccinia striiformis* f. sp. *Tritici*, *PsbO*, *WKS1*, chlorosis, photosynthesis rate, disease resistance, ROS

INTRODUCTION

Wheat stripe rust (or yellow rust, Yr), caused by (*Puccinia striiformis* f. sp. *tritici*, henceforth *Pst*), has been the most substantial biotrophic challenge to wheat production since the last two decades (Schwessinger, 2017). Nowadays, *Pst* is threatening wheat yield in all the major wheat-producing countries across geographical regions, especially those regions with cool and moist weather (Ali et al., 2017). Currently, 5.47 million tons of wheat are lost to the pathogen annually, and this equals to an estimated market value of $USD 1 billion (Beddow et al., 2015). To feed a growing human population and to improve the food supply for the current world population growth (FAOSTAT, 2017), it's essential to reduce yield losses caused by *Pst* (Chen et al., 2014). Reducing yield losses caused by fungal diseases is an efficient avenue for increasing wheat production. Although chemical control is available for wheat fungal pathogens, planting resistant cultivars is a more cost-effective and environmentally friendlier alternative (Ellis et al., 2014).

All stage resistance (ASR) and adult plant resistance (APR) genes are the two major types of fungal resistance genes (Chen, 2017). Compared with ASR, APR genes have a broader spectrum and therefore, are preferred in breeding programs (Lowe et al., 2011). The combination of 4~5 APR genes is usually sufficient to achieve the right level of resistance (Pilet-Nayel et al., 2017; Singh et al., 2000). In the past decade, eight stripe rust resistance genes were successfully cloned, including four nucleotide-binding (NB) and leucine-rich repeat (LRR) genes (*Yr5*, *Yr7*, *YrSP* and *YrAS2388R*), one ASR gene (*Yr15*) and three APR genes (*Yr18*, *Yr36*, and *Yr46*) (Fu et al., 2009; Klymiuk et al., 2018; Krattinger et al., 2009; Marchal et al., 2018; Moore et al., 2015; Zhang et al., 2019). In *Yr15* isogenic lines, large chlorotic blotches with clear HR visible to naked eyes were observed in leaves inoculated with *Pst* (Klymiuk et al., 2018). YR18 resembled an adenosine triphosphate-binding cassette transporter and stimulated senescence-like processes in flag leaves (Krattinger et al., 2009). In rice, *Yr18* transgenic lines developed a typical, senescence-based leaf tip necrosis (LTN) phenotype. *Yr46* (also known as *Pm46*, *Sr55*, and *Ltn3*) encoded a recently evolved hexose transporter localized in the plasma membrane and responded to multiple pathogens with pleiotropic effects including LTN (Moore et al., 2015). In WT plants with *YrAS2388R* gene, necrotic lesions coexisted with resistance phenotype in response to *Pst* (Zhang et al., 2019). In wheat, LTN has been used as a trait linked with durable rust resistance genes (Shah et al., 2011), but the regulatory mechanisms remain elusive.

Yr36 is a high-temperature adult-plant partial resistance gene effective against new races of the *Pst* pathogen that are threatening global wheat production (Uauy et al., 2005). *Yr36* encodes a protein that has a combination of serine/threonine kinase and steroidogenic acute regulatory protein-related lipid-transfer (START) domains and was therefore named *Wheat Kinase START 1* (*WKS1*) (Fu et al., 2009). The full-length transcript encoded protein, WKS1.1, undergoes an N-terminal truncation, enters the chloroplast, and binds and phosphorylates a thylakoid-associated ascorbate peroxidase (tAPX) protein. This phosphorylation inhibits tAPX activity, which leads

to the gradual accumulation of reactive oxygen species (ROS) and eventually, cell death several weeks later (Gou et al., 2015).

Before the increases in ROS, premature chlorosis contributes to fungal resistance, but the molecular mechanism is unknown. In this study, we show that this early chlorosis is associated with the WKS1 phosphorylation of PsbO, one of the subunits of the three extrinsic proteins (PsbO, PsbP and PsbQ) of the Photosystem II (PSII) supercomplex (Ferreira et al., 2004; Liu et al., 2004; Loll et al., 2005; Wei et al., 2016). This hypothesis was confirmed by inducing chlorosis and reduced *Pst* growth in a *psbo-A1* mutant and plants with reduced *PsbO* expression by RNA interference (RNAi). Our biochemical studies showed that WKS1.1 phosphorylates PsbO in its binding regions with PSII, causing its eviction from the PSII complex to and degradation by aspartic and cysteine proteases. These findings indicate that the WKS1.1 phosphorylation of PsbO works as a switch to perturb PSII function, inducing chlorosis and, reduced *Pst* growth.

RESULTS

WKS1.1 Physically Interacts with PsbO in Chloroplasts

Using a previously tested tagged P_{ubi}:*TAP-WKS1.1* (encoding the full-length transcript) transgenic line (Gou et al., 2015), we performed a coimmunoprecipitation (coIP) experiment using soluble protein from fully expanded leaves that were not inoculated with *Pst* and observed that PsbO co-precipitated with WKS1.1 (Supplemental Figure 1). PsbO disruption by a T-DNA insertion or degradation mediated *via* an interacting partner, CV1, is associated with chlorosis in Arabidopsis (Lundin et al., 2008; Wang and Blumwald, 2014). Therefore, we hypothesized that this interaction could be associated with the early chlorosis observed in plants that carried *WKS1* and were infected with *Pst*.

To test this hypothesis, we first checked the binding between WKS1.1 and PsbO in a yeast two-hybrid (Y2H) assay. In yeast, we observed strong interactions between the two full-length proteins, and between PsbO and the WKS1 kinase + interlinker (KI) domains. A relatively weak interaction was detected between PsbO and the WKS1.1 START domain from WKS1.1 (Figure 1A). We then confirmed this interaction via split-luciferase assays. Compared with controls lacking either partner, samples including both WKS1.1 and PsbO displayed a significant increase in luciferase signal (Figure 1B). These data showed that WKS1.1 bound PsbO *in vivo*. Their interaction was further confirmed in a bimolecular fluorescence complementation (BiFC) experiment. In the samples expressing WKS1.1 and PsbO, the fluorescence signal overlapped with the auto-fluorescence signals in the chloroplasts (Figure **1C**). These results were consistent with the chloroplast localization of PsbO-GFP fusion proteins (Supplemental Figure 2), as well as with previous results showing that WKS1.1 could be transported into chloroplasts (Gou et al., 2015; Li et al., 2017).

We further analyzed the localization of WKS1.1 and PsbO inside the chloroplast. A clear signal of WKS1.1 was detected both in the thylakoid membrane and lumen of the wheat chloroplasts (Supplemental Figure 3). The localization in the thylakoid membrane agreed with the earlier report that WKS1.1 had lipid-binding ability and that WKS1.1 phosphorylated the thylakoidal APX protein (Gou et al., 2015). The signal of PsbO was mainly detected in the thylakoid membrane with a faint signal in the lumen, suggesting that the majority of PsbO was bound on the PSII core structure (Supplemental Figure 3).

Overall, the coIP, Y2H, BiFC, and localization experiments supported the hypothesis that WKS1.1 physically interacts with PsbO in wheat chloroplasts.

The *psbo-A1* Mutant Is Resistant to Stripe Rust

To test the effects of PsbO on chlorosis and *Pst* resistance, we isolated a tetraploid wheat ethyl methanesulfonate (EMS) mutant that had a point mutation in a conserved region of PsbO (A genome homolog). The mutant, *psbo-A1* (*Kr1065*), has a serine (aGc=222S) to asparagine (aAc=222N) mutation (Figure 2A). PsbO accumulated at a lower concentration in the *psbo-A1* mutant than in control (Figure 2B). Eighteen days post-inoculation (18 DPI), fewer stripe rust sporulation sites were observed in the *psbo-A1* mutant compared with the wild-type (WT) in the absence of WKS1.1 function (Figure 2C). Both the number of *Pst* sporulation sites (Figure 2D) and the fungal biomass (estimated by the ratio of fungal/host DNA) (Figure 2E) were significantly lower in the *psbo-A1* mutant than in the WT.

To confirm that an increase of *Pst* resistance was caused by the *psbo-A1* mutation, we backcrossed the *psbo-A1*mutant with the wild type Kronos (WT, hereafter). In adult leaf tissues of BC_1F_2 generation plants at Zadoks Growth Scale 18 (Zadoks et al., 1974), the nine plants carrying the *psbo-A1* allele (aAc=222N) showed an improved *Pst* resistance relative to ten plants with the WT allele (aGc=222S) (Figure 2F). Significant reductions in the ratio between *Pst* DNA to host DNA were detected in the nine plants with the *psbo-A1* allele relative to the ten plants with the WT allele (Figure 2G). These data confirmed that the *psbo-A1* mutation allele was linked to the *Pst* resistance phenotype.

To further test the association between *PsbO* and the resistant phenotype, we used RNAi to suppress *PsbO* in the three hexaploid genomes in Fielder transgenic hexaploid wheat lines (Supplemental Figure 4). Figure 2H showed endogenous PsbO protein levels were successfully reduced in the *PsbO* RNAi lines. In these transgenic RNAi lines, we observed a clear reduction in stripe rust growth was detected, which was consistent with the *psbo-A1* mutant phenotype (Figure 2I). The average pustule numbers were significantly lower in the RNAi transgenic lines than in the control plants (Figure 2J). These data support the hypothesis that disruption of *PsbO* increases *Pst* resistance.

Stripe Rust Resistance in the *psbo-A1* Mutant Is Not Due to H_2O_2 Accumulation

To assess the progress of chlorosis and H_2O_2 accumulation in the *psbo-A1* mutants,

we first compared *Pst* growth and H_2O_2 production in WT plants and *psbo-A1* mutants at early stages (2-week-old plants). At 2 DPI, stripe rust germinated, and the fungi grew in both the *psbo-A1* mutant and WT (Figure 3A). However, the average hyphal area within the *psbo-A1* mutants was 40% lower than in the WT plants (Figure 3B). We then checked the amount of H_2O_2 by using 3,3'-diaminobenzidine (DAB) staining but did not observe any significant differences between the WT and *psbo-A1* mutant (Figure 3C-D). The above data indicated that chlorosis could inhibit *Pst* growth before a difference in differential H_2O_2 accumulation could be detected. In addition, there were no significant differences in cell death areas between the WT and *psbo-A1* mutant (Figure 3E). These results indicated that a differential H_2O_2 accumulation was an unlikely cause of the increase in *Pst* resistance in the *psbo-A1* mutant at 2 DPI.

To test if the chlorosis phenotype observed in the *psbo-A1* mutant (and in the *WKS1*-plants showing chlorosis) was associated with reduced photosynthesis, we measured photosynthesis rates in the *psbo-A1*mutant. In a growth chamber experiment, we observed a very significant reduction in the maximal photochemical efficiency of PSII (*Fv*/*Fm*) in the *psbo-A1* mutant relative to the WT (Figure 3F, $P < 0.0001$). Interestingly, the CO_2 assimilation rate was significantly reduced in the *psbo-A1* mutant compared with WT at the jointing stage (Z18 in Zadoks Growth Scale) (Figure 3G, $P < 0.0001$). A similar reduction was also monitored in the *psbo-A1* mutant at the full boot stage (Z38 in Zadoks Growth Scale) (Figure 3H, $P < 0.0001$).

This reduction was in agreement with the observation that, compared with those of the WT plants, the bottom the leaves of the *psbo-A1*mutants displayed an early-chlorosis phenotype (Figure 3I, 3J). An early-chlorosis phenotype was also observed in the transgenic plants suppressing endogenous *PsbO* by RNAi (Figure 3K). In these PsbO RNAi lines, reductions in the maximal photochemical efficiency of PSII (*Fv*/*Fm*) and CO_2 assimilation rate were also detected (Figure 3L-N). Therefore, the increased resistance in the *psbo-A1* mutant and RNAi lines was associated with the changes in photosynthetic rates.

Accelerated leaf chlorosis has also been observed in *WKS1*-mediated *Pst* resistance (Gou et al., 2015). To determine whether there was any change similar to that observed in the *psbo-A1* mutant, we measured photosynthesis rate in *WKS1* transgenic plants under its natural promoter (Gou et al. 2015). The bottom leaves of these transgenic plants showed reductions in the maximal photochemical efficiency of PSII that were significant in two out of the three transgenic plants analyzed (Supplemental Figure 5). Based on this data and the WKS1-PsbO protein interaction described above (Figure 1), we hypothesized that post-transcriptional regulation of PsbO could play a role in the photosynthesis changes observed in the *WKS1* transgenic plants.

WKS1.1 Phosphorylates PsbO on the PSII Docking Face

We previously demonstrated that WKS1.1 phosphorylates tAPX in the thylakoids

(Gou et al., 2015), so we studied the ability of WKS1.1 to phosphorylate PsbO. We first checked phosphorylation using recombinant proteins in conjunction with Q-Diamond, a dye widely used to stain phosphorylated proteins (Jin and Gou, 2016). Upon the initiation of kinase reactions with ATP, a strong phosphorylation signal was detected in the samples with PsbO and WKS1.1, compared with the negative control samples that lacked the ATP needed to initiate the kinase reaction (Figure 4A). In a subsequent experiment, radioactive γ-P^{32}-ATP was supplied in the sample to transfer P^{32} groups to targets during the kinase reaction. After separation by SDS-PAGE, a clear radio-autography band was observed at the PsbO position (Figure 4B). In addition, an auto-phosphorylation band of WKS1.1 was observed (Figure 4B), which is consistent with the results of previous results (Gou et al., 2015).

To understand the phosphorylation process, we evaluated the phosphorylation of PsbO using an anti-phosphorylated threonine-specific (anti-thr^{p}) antibody. A relatively strong signal was detected in the sample with the kinase reaction, but only a very faint signal was detected in the control that lacked ATP (Figure 4C-D). These results indicated that threonine residue(s) in PsbO was (were) phosphorylated by the protein kinase activity of WKS1.1.

The phosphorylated samples were further separated by SDS-PAGE with Phos-tag, which can specifically bind and slow phosphorylated proteins during electrophoresis (Gou et al., 2015). In the sample with the kinase reaction, two relatively slow bands of phosphorylated PsbO were detected (Figure 4E), indicating the presence of multiple phosphorylated sites within PsbO.

To obtain information on putative PsbO phosphorylation sites catalyzed by WKS1.1, we analyzed the phosphorylated samples by mass spectrometry. Phosphorylation was detected on one serine located within the chloroplast transportation signal of PsbO (Figure 4F). However, this amino acid phosphorylation may have little biological effect because this signal peptide is truncated for the formation of mature PsbO in chloroplasts (Ko and Cashmore, 1989). Surprisingly, four amino acids (Thr^{102}, Thr^{104}, Ser^{229}, and Thr^{245}) in two PSII-stabilizing loops (Bommer et al., 2016) were detected as being phosphorylated (Figure 4G). Thr^{102} and Thr^{104} are found in the conserved plant E-rich region, while Ser^{229} and Thr^{245} are located in the conserved C-terminal part of the W region, all of which are on the docking face of PsbO with CP43 in the oxygen evolving-complex (OEC) (De Las Rivas and Barber, 2004) (Figure 4G).

Together, the above results indicate that WKS1.1 can phosphorylate PsbO in regions important for the docking of PsbO with the PSII core complex (Del Val and Bondar, 2017). We hypothesized that phosphorylation of these amino acid residues in this region could alter charges within the docking face, which in turn could affect the binding of phosphorylated PsbO to the PSII complex.

Phosphorylated PsbO Shows Weak Affinity for PSII and Is Rapidly Degraded by Proteases

Phosphorylation is a common post-transcriptional modification for several PSII members such as D1, CP43, PsbH, and LHCII, which are phosphorylated at their N-terminal threonine residues close to the thylakoid stroma side (Grabsztunowicz et al., 2017). Phosphorylation of PSII proteins is induced by light and redox and affects the structure of the complex and protein turnover (Bonardi et al., 2005). The biological consequences of phosphorylation of PsbO, however, have not yet been elucidated.

We further determined the possible effects of PsbO phosphorylation on its binding to the PSII core complex. Recombinant phosphorylation simulation mutants (T^{102E}, T^{104E}, S^{229E}, and T^{245E}) were applied in a PSII recruitment experiment *in vitro* with wheat PSII without PsbO (Figure 5A). Among the single-point mutations, T^{104E} and T^{245E} reduced the binding of PsbO to PSII by approximately 50% on average in three independent experiments, while T^{102E} and S^{229E} did not significantly reduce the binding (Figure 5B). These data indicated that the phosphorylation events at T^{104} and T^{245E} were the most likely to reduce the binding of PsbO to PSII.

We next analyzed the putative effects of PsbO phosphorylation by WKS1.1 on the turnover rate of PsbO. The dynamics of PsbO protein degradation were investigated in wheat extracts from *WKS1* transgenic lines or Bobwhite (BW) controls. The PsbO protein alone showed a strong band after one h in total protein extracts from BW within the same leave number at the same developmental stage (Figure 5C). However, in the samples from the bottom leaves of 6-week-old plants expressing the *WKS1* transgene, PsbO protein was below our detection threshold after half an hour of incubation (Figure 5C), indicating an accelerated turnover of PsbO in the presence of WKS1.1. In addition, faster turnover of PsbO was observed in the presence of exogenous recombinant WKS1.1 protein added in BW (Figure 5C). These results suggested that an accelerated turnover rate of the recombinant PsbO-His fusion protein occurred in the presence of WKS1.1.

To investigate the fate of endogenous PsbO in the transgenic plants accumulating WKS1.1, the protein level of PsbO was compared between the transgenic and BW control plants. In BW, PsbO was detected in the distal portion of the bottom leaves (Figure 5D). However, in the bottom leaves of the transgenic plants, PsbO was below our detection threshold in five out of six samples, and the only exception displayed a weak band (Figure 5D). Interestingly, CP43, the binding partner of PsbO in PSII within the phosphorylated residues (Supplemental Figure 6), was also below our detection threshold (Figure 5D), which is consistent with a previous report in which PsbO protected CP43 from hydrolysis (Lundin et al., 2007).

We finally analyzed the degradation process in more detail. The degradation of PsbO was repeated in the presence of inhibitors against different proteases or proteasomes. In the *WKS1* transgenic plants, only a very faint band of PsbO was detected after 1 hour of degradation. In addition, in the *WKS1* transgenic samples, relatively more residual PsbO was detected in the presence of E64 (a cysteine protease inhibitor), leupeptin (Leu, a threonine, serine, and cysteine protease

inhibitor), NEMI (a cysteine protease inhibitor), or pepstatin A (Peps, an aspartic protease inhibitor), indicating that cysteine and aspartic proteases were involved in PsbO degradation (Figure 5E). In contrast, bestatin (Best, an arginine and alanine peptidase inhibitor) and aprotitin (Apro, a serine protease inhibitor) had little effect on the degradation process. Interestingly, the PsbO signal was even lower in the sample treated with MG132, than in the control sample treated with dimethyl sulfoxide (DMSO) (Figure 5E), which excludes the involvement of the ubiquitin-mediated proteasome pathway in the degradation of PsbO.

Together, our results indicate that phosphorylated PsbO was degraded faster than the nonphosphorylated form and that cysteine and aspartic proteases were likely involved in this degradation. The effects of phosphorylation and accelerated degradation on total PsbO content were similar to those observed in the *psbo-A1* mutants or RNAi transgenic plants.

DISCUSSION

This study identified PsbO as an important interactor of the stripe rust resistance protein WKS1.1. The WKS1-mediated phosphorylation and degradation of PsbO results in reduced photosynthesis rates, induced chlorosis, and a reduced ability of the *Pst* pathogen to grow within leaves. This process preceded by approximately one week the WKS1.1-mediated induction of ROS described previously (Gou et al., 2015).

Our experiments demonstrated that a mutation in *psbo-A1* was sufficient to reduce photosynthesis rates and increase *Pst* resistance at low temperature by reducing the photosynthesis rate, before any significant increase in H_2O_2 accumulation (Figure 3). The effect of the *psbo-A1* mutation was similar to the phosphorylation of PsbO by WKS1.1 (Figure 5). The WKS1-mediated phosphorylation of PsbO occurs after *Pst* infection, minimizing yield losses in the absence of the pathogen (Uauy et al., 2005). In summary, these and previous results indicate that WKS1 regulates *Pst* resistance by phosphorylating a series of downstream targets that first induce chlorosis by phosphorylation of PsbO and later induces the gradual accumulation of ROS and cell death by phosphorylation of tAPX.

PsbO is an extrinsic protein of the PSII complex that facilitates the reception of signals from multiple chlorosis-accelerating proteins, e.g., TGB3 and CV1(Jang et al., 2013; Wang and Blumwald, 2014). Our study adds WKS1.1 to this list. Phosphorylation of PsbO was also detected in rice upon bacterial blight infection (Hou et al., 2016), suggesting that this modification could be conserved in some plant-fungal responses. Phosphorylation in the PsbO docking region can reduce the binding of PsbO to the PSII complex, and accelerated degradation, as shown by the T^{104E} and T^{245E} mutations. This phenomenon would lead to the accumulation of naked PSII, which releases O_2^- instead of O_2(Krieger-Liszkay et al., 2008). O_2^- can be converted to H_2O_2, which could accumulate in chloroplasts in the presence of

WKS1.1, which also phosphorylates and inhibits tAPX activity, reducing the detoxification mechanisms for ROS (Gou et al., 2015). Accumulated H_2O_2 could further oxidize PsbO to destabilize the disulfate bound between PsbO and accelerate PsbO degradation (Hall et al., 2010).

Leaf necrosis, including leaf tip necrosis (LTN), necrosis lesions or large chlorotic blotches, was reported in rust responses of several cloned *Pst* resistance genes, including *Yr15*, *Yr18* and *Yr46* and *YrAS2388* (Klymiuk et al., 2018; Krattinger et al., 2009; Moore et al., 2015; Zhang et al., 2019). These genes encode different classes of proteins, including protein kinase (Klymiuk et al., 2018), ABC transporter (Krattinger et al., 2009) and hexose transporter (Moore et al., 2015). Despite differences among their biochemical characteristics and subcellular localization, these genes could share conserved physiological changes (H_2O_2 accumulation and degradation processes in chloroplasts) with WKS1. It's interesting to explore potential changes and regulations of key elements, e.g., PsbO and tAPX, discovered here and previously (Gou et al., 2015), in other plant resistant pathogenic responses.

Based on the sub-organelle localization of WKS1.1 and PsbO, it is very likely that the phosphorylation of PsbO by WKS1.1 occurred in the thylakoid, ether in the lumen or in the thylakoid membrane. However, we cannot exclude the possibility that PsbO phosphorylation occurs at components different than the thylakoid.

In summary, we propose that the phosphorylation of PsbO by WKS1 reduces the binding affinity of the former with the PSII core complex and accelerates PsbO degradation. These perturbations in PsbO negatively affect the photosynthesis rate, induce chlorosis and generate an unfavorable environment for *Pst* growth, which is further controlled later by the phosphorylation of tAPX and induced cell death (Figure 6). This set of events coordinated by WKS1.1 provides resistance to a broad spectrum of *Pst* races.

METHODS

Plant Materials and Growth Conditions

The transgenic hexaploid *WKS1* lines (26B6, 26B15, 17A4, 17A15, and P_{Ubi}:*TAP-WKS1.1*) in the Bobwhite (BW) background were described previously (Gou et al., 2015). The PsbO EMS A genome mutant (*psbo-A1*, *Kr1065*, S222N) was identified in the sequenced mutant population of the tetraploid wheat variety Kronos (Krasileva et al., 2017). The A and B genomes of Kronos encode identical proteins, but the transcript levels of *PsbO-A1* are two-fold higher than those of *PsbO-B1* (paired *t*-test $P = 2.6\ E^{-11}$, based on 30 RNAseq studies in leaves from http://www.wheat-expression.com/).

The *PsbO* RNAi transgenic lines in Fielder were transformed by agro with construct vector pANDA (Miki and Shimamoto, 2004), including an inverted repeat of 643 bps (from position 323 to 965) in the cDNA of *PsbO-A1*. This region included tracks of more than 21-bp that are identical in all three genomes and is expected to

down-regulate all the three *PsbO-A1* homeologs.

All the plants were grown in a growth chamber at 22 °C, under 65% relative humidity and 200 mmol m^{-2} s^{-1} intensity white light for a 16-hour photoperiod. Both the transgenic and EMS segregating mutants were evaluated in at least two generations.

Puccinia striiformis f. sp. _tritici_ Inoculations

Spores of the *Pst* race *CR32* were increased in the wheat cultivar *SY11* in a growth chamber at 15°C and 80% relative humidity (RH). *Pst* inoculated plants were grown for two weeks in the host plant and then used to collect spores. Fresh spores were compiled into a 1.5 ml tube and spread onto the top of a water drop in a petri dish. An equal volume was spread with a needle onto the middle region of the sheaths. The infected plants were kept in the dark for 24 h and then grown under a 16-h photoperiod until analysis. At two days post-inoculation (DPI), the hyphal area, ROS accumulation, and cell death area were stained with wheat germ agglutinin conjugated to Alexa-488 (Invitrogen, Waltham, MA) and DAB (Ayliffe et al., 2011), respectively. At 18 DPI, the pustule number was counted, and biomass was analyzed using DNA extracted from the infected region to compare *PstEF1* with wheat *EF1α* (Cheng et al., 2015). Total DNA was extracted from adult leaves of segregating BC_1F_2 plants at Zadoks Growth Scale Z18 (Zadoks et al., 1974). Plants were genotyped by PCR with gene-specific primers and Sanger sequencing (Sangon, Shanghai, China). Three different BC_1F_3 lines were used for pustule number count and rust biomass quantification, each with four biological repeats.

CoIP and Y2H Assays

Total protein was extracted from leaves of P_{Ubi}:*TAP-WKS1.1* transgenic plants overexpressing WKS1.1 with plant protein extraction buffer (100mM Tris-HCl pH 7.5, 300mM NaCl, 2mM EDTA, 1%Triton X-100, 10% glycerol, 1/100 v/v Protease Inhibitor Cocktail). Forty ml of the above extract were mixed with 100 µl of IgG Sepharose beads (Amersham Biosciences, Piscataway, NJ, USA), and were kept in ice for one h. Beads were collected by centrifugation at 200g for 3 min at 4 °C, and washed three times with ice-cold extraction buffer following two washes with Tobacco Etch Virus (TEV) protease (TEV) digestion buffer (10 mM Tris–HCl pH 8.0, 150 mM NaCl, 0.1% IGEPAL, 0.5 mM EDTA, 1 mM DTT). TAP-tagged proteins were released by digestion with 30 µl TEV protease (300-500 U; Invitrogen, ThermoFisher, Shanghai, China) for 1 h at 16 °C. The TEV cleaved eluate was adjusted to 2 mM $CaCl_2$ and diluted with 3 volumes of calmodulin-binding buffer (CBB: 10 mM b-mercaptoethanol; 10 mM Tris–HCl pH 8.0; 150 mM NaCl; 1 mM Mg-acetate; 1 mM imidazole; 2 mM CaCl2; 0.1% IGEPAL) . The final volume was adjusted to 1 ml and incubated with 100µl of calmodulin-agarose beads (Stratagene, La Jolla, CA, USA) for 1 h at 4 °C to collect the WKS1.1 protein complex (Gou et al., 2015). The eluted proteins were precipitated with trichloroacetic acid, separated by SDS-PAGE and subjected to mass spectral analyses.

Cloning of the different fragments of *WKS1.1* in the Gateway-compatible AD

vector pLAW11 was described previously (Gou et al., 2015). *PsbO –A1*full length cDNA in an entry vector was then inserted into the Gateway-compatible BD vector pLAW10 by LR clonase II (11791100, Invitrogen, ThermoFisher, Shanghai, China). The plasmids were transformed into Y187 and Y2H Gold yeast cells by a LiAc mediated transformation procedure according to the Clontech user manual. Mating and yeast growth were performed as described in the Clontech user manual.

Photosynthesis Measurements

Third leaves in plants at both stages Z18 and Z38 in the Zadoks Growth Scale (Zadoks et al., 1974) were selected for analysis of their photosynthetic characteristics and photosynthetic efficiency in growth chamber experiments. CO_2 assimilation rates were analyzed with a Li-COR 6400 using a 6 cm^2 fluorescent pad (LI-COR Corporate, Lincoln, Nebraska USA). The flow of CO_2 flow was set to 400 $\mu mol \cdot mol^{-1}$, the RH was set to 50~75%, and the fan speed was 10,000 rpm. The fluorometer was in "Control Mode" with a setpoint of 1500 $\mu molm^{-2}s^{-1}$. At least eight plants from each sample were analyzed at a similar position on the same leaf. The *Fv*/*Fm* was quantified with Li-COR 6400, according to the manufacturer's instructions (LI-COR Corporate).

Split-luciferase Assays, Subcellular Localization, and BiFC Assays

WKS1.1 and *PsbO* were incorporated into a Gateway-compatible split-luciferase system using protoplast transient transformation and then monitored with a plate reader (Fujikawa and Kato, 2007). *PsbO* was incorporated into pMDC83 (Curtis and Grossniklaus, 2003), which was subsequently infiltrated into tobacco leaves and then observed under a Leica TCS SP8 (Leica, Microsystems, Mannheim, Germany). Images were captured at 488-nm laser excitation and 500-to 550-nm long-pass emission filters. Chloroplast autofluorescence was imaged at 600-nm over a long pass emission filter.

WKS1.1 and *PsbO* were incorporated into a BiFC system (Bracha-Drori et al., 2004), which was then infiltrated into tobacco leaves and subsequently observed under a confocal microscope. For the *in vivo* binding of PsbO with CP43, the CDS of *CP43* (ATCG00280) and PsbO without the signal peptide were cloned into Firefly luciferase complementation imaging vectors, pCAMBIA-NLuc and pCAMBIA-CLuc (Arabidopsis Biological Resource Center), respectively. FAD2 (AT3G12120) with the polymerization ability was used as a positive control (Lou et al., 2014).

WT plants at Z15 stage in a growth chamber at short-day conditions were used to extract different fractions of chloroplast modified from a published protocol (Hall et al., 2011). The leaves (20 g) were ground in 170 ml of chloroplast extraction buffer (20 mM Tris-HCl pH8.4, 300 mM sorbitol, 10 mM KCl, 10 mM EDTA, 0.25% (w/v) bovine serum albumin (BSA), 4.5 mM sodium ascorbate, and 5 mM, L-cysteine) in a 4 °C cold room. Intact chloroplasts were extracted using Percoll (40501ES60, Yeasen, Shanghai China) gradient centrifugation according to our previous publication (Gou et al., 2015). The intact chloroplasts were diluted with osmotic-shocking buffer (10 mM Na-pyrophosphate-NaOH, pH7.8) to the final concentration of chlorophyll (Chl) to

0.2 mg Chl/ml. The samples were passed through a 10 ml syringe three times, homogenized once in a 40-ml glass homogenizer and centrifuged at 7,500g for 5 min at 4 °C to pellet thylakoids. The supernatant was centrifuged at 100,000g for 1h at 4 °C to collect the supernatant as crude stroma. The crude stroma sample was further concentrated into 200 µl and saved as stroma fraction in -80 °C until further analysis. The thylakoids were resuspended in 25 ml of osmotic buffer and further washed twice with ice-cold thylakoid wash buffer II (2 mM Tris-HCl pH7.8, 300 mM sucrose). The thylakoids were adjusted to 3~4 mg/ml Chl and broken at 100 bar twice in a Yeda press chamber. The fragmented thylakoid membrane was pelleted by centrifugation at 200, 000g for 1h at 4 °C. The supernatants were transferred to a new tube, centrifuged at 200, 000g for 1h at 4 °C and concentrated to 200µl in a 10 kDa ultrafiltration tube (Millipore，Sigma) to collect lumen fraction. The above samples were separated on SDS-PAGE and analyzed their WKS1 content with a rabbit polyclonal anti-WKS1 antibody generated in this study using full-length WKS1 in a local company (Abmart, Shanghai China). Goat anti-rabbit IgG HRP (Abmart) was used as the secondary antibody, according to the manufacturer user manual.

Protein Phosphorylation

The full-length coding sequences of PsbO and WKS1.1 were inserted into pET28a (His6-PsbO-His6) and pET41b (GST-His6-WKS1-His6) vectors, respectively, which were then transformed into Rosetta through heat-shock. During protein expression induced by 0.5 mM isopropyl β-D-1-thiogalactopyranoside (IPTG) at 18 °C, n-terminal truncation occurred in WKS1.1 and released mWKS1.1-His6 plus GTS-His-$SP_{WKS1.1}$. GTS-His-$SP_{WKS1.1}$ was removed by glutathione Agarose resin (Pearce, ThermoFisher, Shanghai, China). Recombinant PsbO and the mature form of WKS1.1-His6 (mWKS1.1) were purified according to a previously described procedure (Gou et al., 2009).

PsbO and WKS1.1 (mature protein without the normally removed n-terminal region), 2 mg each (PsbO: WKS1.1=1:1, m:m), with or without radioactive γ-P^{32}-ATP were mixed together at room temperature (RT) for 30 min. The samples were passed through a Zeba™ Spin Desalting Columns, 7K MWCO (Pearce, ThermoFisher, Shanghai, China) to remove unreacted γ-P^{32}-ATP. The eluates were mixed with 1/5 volume of 6X SDS sample buffer, separated by SDS-PAGE and imaged with Typhoon FLA 9000 instrument (GE Healthcare, Waukesha, WI, USA).

Two mg of PsbO was phosphorylated by 0.2 mg of WKS1.1 (PsbO: WKS1.1=10:1, m:m) with cold ATP, stained by Pro-Q™ Diamond Phosphoprotein Gel Stain (P33300, Invitrogen, ThermoFisher, Shanghai, China) for phosphor-fluorescence in the dark for 1 h at room temperature. Proteins were pelleted again with cold acetone and washed three more times with cold acetone to remove the residual stain. Stained proteins were suspended in 200 µl of ddH_2O to quantify the fluorescence using a Synergy 2 (Biotek, Winooski, VT, USA) plate reader (excitation= 488 nm and emission= 595 nm) (Jin and Gou, 2016).

For the phosphorylated amino acid residue type analyses, the reaction products were separated by SDS-PAGE and recognized by anti-phosphorylated threonine

monoclonal antibody (047K4770, Sigma, Thermofisher), and goat anti-mouse IgG HRP (M21001, Abmart) according to the manufacturer user manual. The samples were developed with a basic ECL kit (AB Clonal) in Tanon 5200 Multi imaging system (Tanon Science & Technology Co., Ltd., Shanghai, China).

For the gel retardation assay, the phosphorylated samples were separated in Phos-tag (FUJIFILM Wako Pure Chemical Corporation, Osaka, Japan) containing SDS PAGE (Gou et al., 2015). PsbO was analyzed with anti-PsbO (AS05 092, Agrisera, Vännäs, Sweden). Goat anti-mouse IgG HRP (M21002, Abmart) was used as the secondary antibody according to the manufacturer user manual and developed as described above.

For phosphorylation amino acid residue analyses, the reaction products were analyzed in the core facility *via* MS/MS for phosphorylated amino acid residues. The Phosphorylation sites were highlighted in a structural model of PsbO in a dark state X-ray diffraction of PSII (4IXQ, PDB, NCBI) (Kern et al., 2013).

For Ponceau staining, the PVDF membrane was submerged in 4 ml of ddH_2O. Then 1 ml of EZ-Buffers F 5X Ponceau S Staining buffer solution (Sangong Biotech, Shanghai, China) was added and kept at RT for 3 min. After a brief washing with ddH_2O, the membrane was visualized in a Tanon 5200 Multi imaging system.

PsbO Degradation and Reconstruction

For *in vivo* degradation, 2 µl (5 µg) of recombinant PsbO was mixed with total protein extract from fully expanded leaves of 2-month-old *WKS1*-transgenic, the Bobwhite control (BW), or BW with 5µg recombinant WKS1.1 for 0, 30 and 60 min at RT. The degradation process was stopped by the addition of 1/5 volume of 6X SDS loading buffer and boiling for 5 min. The PsbO content was monitored using Tag-His-Tag (10E2) mouse monoclonal antibody (M30111, Abmart, Shanghai China) and goat anti-mouse IgG HRP (M21001, Abmart) according to the manufacturer user manual. The samples were developed with a basic ECL kit (AB Clonal) in Tanon 5200 Multi imaging system (Tanon Science & Technology Co., Ltd., Shanghai, China).

For the *in vivo* degradation of endogenous proteins, intact chloroplasts were isolated using Percoll (40501ES60, Yeasen, Shanghai China) gradient centrifugation according to our previous publication (Gou et al., 2015). Endogenous PsbO was analyzed with anti-PsbO (AS05 092, Agrisera, Vännäs, Sweden) and anti-CP43 antibodies generated with peptides from protein homologs from Arabidopsis (AS06 111, Agrisera). Goat anti-mouse IgG HRP (M21002, Abmart) was used as the secondary antibody according to the manufacturer user manual.

To analyze the degradation process, different amounts of inhibitors (1mM Peps, 1 mM Apro, 3 mM Best, 1 mM Leu, 5 mM E-63, 5 mM NEMI, or 50 µM MG132, all from Sigma) in DMSO were supplied in the above digestion buffer for 0, 30, and 60 min at RT before PsbO analyses via anti-HIS antibodies as described above.

For the binding activity assay, wheat OEC was washed with 2.6 M urea plus 200 mM NaCl to remove PsbO according to a previous publication (Miyao and Murata, 1984). Five µg of recombinant PsbO WT and phosphorylation simulation mutant proteins were mixed with an equal amount of wheat OEC without PsbO for 30 min,

centrifuged at 13000 rpm for 10 minutes at 4 °C and then washed three times with reconstruction buffer (Betts et al., 1994). The proteins bound on the complex were analyzed by Western blots in conjunction with anti-HIS antibodies (Abmart) and quantified using ImageJ; 3 different biological repeats were included.

REFERENCES

Ali, S., Rodriguez-Algaba, J., Thach, T., Sorensen, C.K., Hansen, J.G., Lassen, P., Nazari, K., Hodson, D.P., Justesen, A.F., and Hovmoller, M.S. (2017). Yellow Rust Epidemics Worldwide Were Caused by Pathogen Races from Divergent Genetic Lineages. Front Plant Sci *8*, 1057.

Ayliffe, M., Devilla, R., Mago, R., White, R., Talbot, M., Pryor, A., and Leung, H. (2011). Nonhost resistance of rice to rust pathogens. Mol Plant Microbe Interact *24*, 1143-1155.

Beddow, J.M., Pardey, P.G., Chai, Y., Hurley, T.M., Kriticos, D.J., Braun, H.J., Park, R.F., Cuddy, W.S., and Yonow, T. (2015). Research investment implications of shifts in the global geography of wheat stripe rust. Nat Plants *1*, 15132.

Betts, S.D., Hachigian, T.M., Pichersky, E., and Yocum, C.F. (1994). Reconstitution of the spinach oxygen-evolving complex with recombinant Arabidopsis manganese-stabilizing protein. Plant Molecular Biology *26*, 117-130.

Bommer, M., Bondar, A.N., Zouni, A., Dobbek, H., and Dau, H. (2016). Crystallographic and Computational Analysis of the Barrel Part of the PsbO Protein of Photosystem II: Carboxylate-Water Clusters as Putative Proton Transfer Relays and Structural Switches. Biochemistry *55*, 4626-4635.

Bonardi, V., Pesaresi, P., Becker, T., Schleiff, E., Wagner, R., Pfannschmidt, T., Jahns, P., and Leister, D. (2005). Photosystem II core phosphorylation and photosynthetic acclimation require two different protein kinases. Nature *437*, 1179-1182.

Bracha-Drori, K., Shichrur, K., Katz, A., Oliva, M., Angelovici, R., Yalovsky, S., and Ohad, N. (2004). Detection of protein–protein interactions in plants using bimolecular fluorescence complementation. The Plant Journal *40*, 419-427.

Chen, W., Wellings, C., Chen, X., Kang, Z., and Liu, T. (2014). Wheat stripe (yellow) rust caused by Puccinia striiformis f. sp. tritici. Mol Plant Pathol *15*, 433-446.

Chen, X.M., Kang, Z.S., ed. (2017). Stripe Rust (Springer Nature).

Cheng, Y., Wang, X., Yao, J., Voegele, R.T., Zhang, Y., Wang, W., Huang, L., and Kang, Z. (2015). Characterization of protein kinase PsSRPKL, a novel pathogenicity factor in the wheat stripe rust fungus. Environ Microbiol *17*, 2601-2617.

Curtis, M.D., and Grossniklaus, U. (2003). A gateway cloning vector set for high-throughput functional analysis of genes in planta. Plant Physiol *133*, 462-469.

De Las Rivas, J., and Barber, J. (2004). Analysis of the Structure of the PsbO Protein and its Implications. Photosynthesis Research *81*, 329-343.

Del Val, C., and Bondar, A.N. (2017). Charged groups at binding interfaces of the PsbO subunit of photosystem II: A combined bioinformatics and simulation study. Biochim Biophys Acta Bioenerg *1858*, 432-441.

Ellis, J.G., Lagudah, E.S., Spielmeyer, W., and Dodds, P.N. (2014). The past, present and future of breeding rust resistant wheat. Front Plant Sci *5*, 641.

Ferreira, K.N., Iverson, T.M., Maghlaoui, K., Barber, J., and Iwata, S. (2004). Architecture of the photosynthetic oxygen-evolving center. Science *303*, 1831-1838.

Fu, D., Uauy, C., Distelfeld, A., Blechl, A., Epstein, L., Chen, X., Sela, H., Fahima, T., and Dubcovsky, J.

(2009). A kinase-START gene confers temperature-dependent resistance to wheat stripe rust. Science *323*, 1357-1360.

Fujikawa, Y., and Kato, N. (2007). Split luciferase complementation assay to study protein-protein interactions in Arabidopsis protoplasts. Plant J *52*, 185-195.

Gou, J.Y., Li, K., Wu, K., Wang, X., Lin, H., Cantu, D., Uauy, C., Dobon-Alonso, A., Midorikawa, T., Inoue, K.*, et al.* (2015). Wheat Stripe Rust Resistance Protein WKS1 Reduces the Ability of the Thylakoid-Associated Ascorbate Peroxidase to Detoxify Reactive Oxygen Species. Plant Cell *27*, 1755-1770.

Gou, J.Y., Yu, X.H., and Liu, C.J. (2009). A hydroxycinnamoyltransferase responsible for synthesizing suberin aromatics in Arabidopsis. Proc Natl Acad Sci U S A *106*, 18855-18860.

Grabsztunowicz, M., Koskela, M.M., and Mulo, P. (2017). Post-translational Modifications in Regulation of Chloroplast Function: Recent Advances. Front Plant Sci *8*, 240.

Hall, M., Mata-Cabana, A., Akerlund, H.E., Florencio, F.J., Schroder, W.P., Lindahl, M., and Kieselbach, T. (2010). Thioredoxin targets of the plant chloroplast lumen and their implications for plastid function. Proteomics *10*, 987-1001.

Hall, M., Mishra, Y., and Schroder, W.P. (2011). Preparation of stroma, thylakoid membrane, and lumen fractions from Arabidopsis thaliana chloroplasts for proteomic analysis. Methods Mol Biol *775*, 207-222.

Hou, Y., Tong, X., Wang, Y., Qiu, J., Li, Z., Zhang, W., Huang, S., and Zhang, J. (2016). Data set from a comprehensive phosphoproteomic analysis of rice variety IRBB5 in response to bacterial blight. Data Brief *6*, 282-285.

Jang, C., Seo, E.-Y., Nam, J., Bae, H., Gim, Y.G., Kim, H.G., Cho, I.S., Lee, Z.-W., Bauchan, G., Hammond, J.*, et al.* (2013). Insights into Alternanthera mosaic virus TGB3 Functions: Interactions with Nicotiana benthamiana PsbO Correlate with Chloroplast Vesiculation and Veinal Necrosis Caused by TGB3 Over-Expression. Frontiers in Plant Science *4*.

Jin, X., and Gou, J.Y. (2016). A rapid and cost-effective fluorescence detection in tube (FDIT) method to analyze protein phosphorylation. Plant Methods *12*, 43.

Kern, J., Alonso-Mori, R., Tran, R., Hattne, J., Gildea, R.J., Echols, N., Glockner, C., Hellmich, J., Laksmono, H., Sierra, R.G.*, et al.* (2013). Simultaneous femtosecond X-ray spectroscopy and diffraction of photosystem II at room temperature. Science *340*, 491-495.

Klymiuk, V., Yaniv, E., Huang, L., Raats, D., Fatiukha, A., Chen, S., Feng, L., Frenkel, Z., Krugman, T., Lidzbarsky, G.*, et al.* (2018). Cloning of the wheat Yr15 resistance gene sheds light on the plant tandem kinase-pseudokinase family. Nat Commun *9*, 3735.

Ko, K., and Cashmore, A.R. (1989). Targeting of proteins to the thylakoid lumen by the bipartite transit peptide of the 33 kd oxygen-evolving protein. The EMBO journal *8*, 3187-3194.

Krasileva, K.V., Vasquez-Gross, H.A., Howell, T., Bailey, P., Paraiso, F., Clissold, L., Simmonds, J., Ramirez-Gonzalez, R.H., Wang, X., Borrill, P.*, et al.* (2017). Uncovering hidden variation in polyploid wheat. Proc Natl Acad Sci U S A *114*, E913-E921.

Krattinger, S.G., Lagudah, E.S., Spielmeyer, W., Singh, R.P., Huerta-Espino, J., McFadden, H., Bossolini, E., Selter, L.L., and Keller, B. (2009). A putative ABC transporter confers durable resistance to multiple fungal pathogens in wheat. Science *323*, 1360-1363.

Krieger-Liszkay, A., Fufezan, C., and Trebst, A. (2008). Singlet oxygen production in photosystem II and related protection mechanism. Photosynth Res *98*, 551-564.

Li, Q.P., Wang, S., and Gou, J.Y. (2017). A split ubiquitin system to reveal topology and released

peptides of membrane proteins. BMC Biotechnol *17*, 69.
Liu, Z., Yan, H., Wang, K., Kuang, T., Zhang, J., Gui, L., An, X., and Chang, W. (2004). Crystal structure of spinach major light-harvesting complex at 2.72 A resolution. Nature *428*, 287-292.
Loll, B., Kern, J., Saenger, W., Zouni, A., and Biesiadka, J. (2005). Towards complete cofactor arrangement in the 3.0 A resolution structure of photosystem II. Nature *438*, 1040-1044.
Lou, Y., Schwender, J., and Shanklin, J. (2014). FAD2 and FAD3 desaturases form heterodimers that facilitate metabolic channeling in vivo. J Biol Chem *289*, 17996-18007.
Lowe, I., Cantu, D., and Dubcovsky, J. (2011). Durable resistance to the wheat rusts: Integrating systems biology and traditional phenotype-based research methods to guide the deployment of resistance genes. Euphytica *179*, 69-79.
Lundin, B., Hansson, M., Schoefs, B., Vener, A.V., and Spetea, C. (2007). The Arabidopsis PsbO2 protein regulates dephosphorylation and turnover of the photosystem II reaction centre D1 protein. Plant J *49*, 528-539.
Lundin, B., Nurmi, M., Rojas-Stuetz, M., Aro, E.M., Adamska, I., and Spetea, C. (2008). Towards understanding the functional difference between the two PsbO isoforms in Arabidopsis thaliana--insights from phenotypic analyses of psbo knockout mutants. Photosynth Res *98*, 405-414.
Marchal, C., Zhang, J., Zhang, P., Fenwick, P., Steuernagel, B., Adamski, N.M., Boyd, L., McIntosh, R., Wulff, B.B.H., Berry, S.*, et al.* (2018). BED-domain-containing immune receptors confer diverse resistance spectra to yellow rust. Nat Plants *4*, 662-668.
Miki, D., and Shimamoto, K. (2004). Simple RNAi vectors for stable and transient suppression of gene function in rice. Plant Cell Physiol *45*, 490-495.
Miyao, M., and Murata, N. (1984). Role of the 33-kDa polypeptide in preserving Mn in the photosynthetic oxygen-evolution system and its replacement by chloride ions. FEBS Letters *170*, 350-354.
Moore, J.W., Herrera-Foessel, S., Lan, C., Schnippenkoetter, W., Ayliffe, M., Huerta-Espino, J., Lillemo, M., Viccars, L., Milne, R., Periyannan, S.*, et al.* (2015). A recently evolved hexose transporter variant confers resistance to multiple pathogens in wheat. Nat Genet *47*, 1494-1498.
Pilet-Nayel, M.L., Moury, B., Caffier, V., Montarry, J., Kerlan, M.C., Fournet, S., Durel, C.E., and Delourme, R. (2017). Quantitative Resistance to Plant Pathogens in Pyramiding Strategies for Durable Crop Protection. Front Plant Sci *8*, 1838.
Schwessinger, B. (2017). Fundamental wheat stripe rust research in the 21(st) century. New Phytol *213*, 1625-1631.
Shah, S.J.A., Hussain, S., Ahmad, M., Farhatullah, Ali, I., and Ibrahim, M. (2011). Using leaf tip necrosis as a phenotypic marker to predict the presence of durable rust resistance gene pair Lr34/Yr18 in wheat. J Gen Plant Pathol *77*, 174-177.
Singh, R., Huerta-Espino, J., and Rajaram, S. (2000). Achieving Near-immunity to Leaf and Stripe Rusts in Wheat by Combining Slow Rusting Resistance Genes, Vol 35.
Uauy, C., Brevis, J.C., Chen, X., Khan, I., Jackson, L., Chicaiza, O., Distelfeld, A., Fahima, T., and Dubcovsky, J. (2005). High-temperature adult-plant (HTAP) stripe rust resistance gene Yr36 from Triticum turgidum ssp. dicoccoides is closely linked to the grain protein content locus Gpc-B1. Theor Appl Genet *112*, 97-105.
Wang, S., and Blumwald, E. (2014). Stress-induced chloroplast degradation in Arabidopsis is regulated via a process independent of autophagy and senescence-associated vacuoles. Plant Cell *26*, 4875-4888.

Wei, X., Su, X., Cao, P., Liu, X., Chang, W., Li, M., Zhang, X., and Liu, Z. (2016). Structure of spinach photosystem II-LHCII supercomplex at 3.2 A resolution. Nature *534*, 69-74.

Zadoks, J.C., Chang, T.T., and Konzak, C.F. (1974). A decimal code for growth stages of cereals. Weed Res *14*, 7.

Zhang, C., Huang, L., Zhang, H., Hao, Q., Lyu, B., Wang, M., Epstein, L., Liu, M., Kou, C., Qi, J.*, et al.* (2019). An ancestral NB-LRR with duplicated 3'UTRs confers stripe rust resistance in wheat and barley. Nat Commun *10*, 4023.

SUPPLEMENTAL INFORMATION

Supplemental Information includes Supplemental Figures 1-6.

FUNDING

The research described here is supported by the National Key R&D Program of China (2016YFD0100500) and the National Science Foundation of China (NSFC) (31772146, 31972350) for J.G. JD acknowledges support from BARD and the Howard Hughes Medical Institute. We thank an open project support from the National Key Laboratory of Wheat and Maize Crop Science, Henan Agricultural University.

AUTHOR CONTRIBUTIONS

J. G. designed the experiment. S. W. and Q. L. performed most of the experiments. J.W., X. W. and K. Z. carried out the stripe rust infections. Y. Y., G. Z., and F.C. analyzed the stripe rust infection results. Y. Y., H. Z., and J. W. prepared the transgenic wheat. J. D. generated the EMS mutants. J. D. and J. G. analyzed the data and wrote the paper. All authors reviewed the manuscript.

FIGURE LEGENDS

Figure 1. WKS1 Binds PsbO in the Chloroplast

(A) Direct binding between PsbO and different fragments of WKS1.1. KA, kinase domain alone. KI, kinase domain and inter linker. IS, inter linker and START domain. SA, START domain alone. FL, full-length WKS1.1. -, empty vector control.

(B) Complemented *Renilla* luciferase activities in plant cells. RFU, relative fluorescence unit. H2A and H2B, positive controls. An6 and Dn6, empty vector negative controls. n=4, *** Student's t-test $P < 0.001$. Bars = ±SE.

(C) WKS1.1 binds PsbO in the chloroplast.

(D-E) Empty vector controls without fluorescence signals. The bars represent 50 μm.

Figure 2. The PsbO Mutation Increases Stripe Rust Resistance

(A) Position of the point mutation within the *psbo-A1* mutant.

(B) PsbO protein levels in WT (Kronos, hereafter) and *psbo-A1* mutant. The bands in the *psbo-A1* mutant likely correspond to the *PsbO-B1* homeolog, which is expressed at half the levels of *PsbO-A1* and encodes an identical protein. Ponceau staining shows the contents of the large unit of RuBisCo in the samples.

(C) Growth of *Pst* in WT and *psbo-A1* mutant.

(D) Number of *Pst* pustules in WT and *psbo-A1* mutant. n= 12.

(E) *Pst*/ host DNA rates in WT and *psbo-A1* mutant estimated by comparing the relative contents of *PstEF1* with those of wheat *EF1α*. n= 12.

(F) Growth of *Pst* in BC_1F_2 segregating plants with WT and the *psbo-A1* alleles, respectively. Only one representative sample out the 10 segregating plants harboring the WT allele is shown.

(G) *Pst*/ host DNA rates in BC_1F_2 segregating plants with WT and *psbo-A1* alleles, respectively.

(H) Levels of endogenous PsbO protein in *PsbO* RNAi transgenic wheat lines. Ponceau staining shows the contents of the large unit of RuBisCo in the samples.

(I) *Pst* growth in WT and *PsbO* RNAi transgenic wheat lines.

(J) Number of *Pst* pustules in Fielder control and *PbsO* RNAi transgenic lines at 16 °C. n= 4.

Student's t-tests: * $P < 0.05$, ** $P < 0.01$. Bars= ± SE.

Figure 3. The *psbo-A1* Mutant Exhibits *Pst* Resistance Before H_2O_2 Accumulation

(A) *Pst* growth in WT and *psbo-A1* mutant at 2DPI (stained with wheat germ agglutinin conjugated to Alexa-488). Bars = 75 μm.

(B) Average *Pst* hyphal area in WT and *psbo-A1* mutant. n = 40.

(C) DAB staining of ROS and cell death in WT and *psbo-A1* mutant. r：ROS region. cd：cell death region. Bars = 40 μm.

(D) Average areas of H_2O_2 in WT and the *psbo-A1* mutant. n = 40.

(E) Average areas of cell death in WT and the *psbo-A1* mutant. n = 40.

(F) Primary light energy conversion efficiencies in WT and *psbo-A1* mutant. n = 8.

(G-H) CO_2 assimilation rates in WT and *psbo-A1* mutant at Z18 (G) and Z38 (H) stages. N = 8.

(I-J) Early-chlorosis phenotype in bottom leaves of *psbo-A1* mutant.

(K) Early-chlorosis phenotype in *PsbO* RNAi transgenic lines.

(L) Primary light energy conversion efficiencies in *PsbO* RNAi lines and controls. n = 8.

(M-N) CO_2 assimilation rates in *PsbO* RNAi lines and Fielder control at Z18 (M) and Z38 (N) stages. N = 8.

Student's t-test: * $P < 0.05$, *** $P < 0.001$. Bars = ± SE.

Figure 4. WKS1 Phosphorylates PsbO at PSII Binding Regions

(A) Phosphor fluorescence signal of PsbO samples after a kinase reaction catalyzed by WKS1.1. tAPX serves as a positive control. Note, PsbO: WKS1.1=10:1, m:m. RFU, relative fluorescence unit. n = 4. Student's *t*-test: *** $P < 0.001$. Bars = ± SE.

(B) Phospho image of PsbO after a kinase reaction initiated by radioactive γ-P^{32}-ATP. Note, PsbO: WKS1.1=1:1, m:m.

(C) Increase in phosphorylated threonine signal on PsbO after kinase reaction.

(D) PsbO content in panel C recognized by an anti-PsbO antibody.

(E) Gel retardation of PsbO after kinase reaction. Note: at least two slowed bands were observed.

(F) Position of phosphorylated amino residues in PsbO. Green, chloroplast signal peptide. Brown, thylakoid transportation signal. Red, phosphorylated amino acids. The red double wave lines mark the binding docking face between PsbO and CP43.

(G) Phosphorylated amino acids in a structural model of PsbO (modified from PDB 4IXQ).

Figure 5. Phosphorylated PsbO Has Weak Affinity for PSII and Is Degraded by Proteinases

(A) Recruitment of PsbO WT and phosphorylation simulations within the PSII core complex.

(B) Quantification of the above PsbO bands in the PSII recruitment experiments. n = 3, Student's *t*-test: ** $P < 0.01$. Bars = ± SE.

(C) Degradation of recombinant PsbO in Bobwhite (BW) and transgenic plants expressing *WKS1.1* (*NP*: *WKS1*), or BW supplemented with recombinant WKS1.1 (BW WKS1.1-His).

(D) Endogenous level of PsbO and CP43 in BW or *WKS1*-transgenic plants.

(E) Effects of protease inhibitors on the degradation process of PsbO. Bobwhite (BW) serves as a negative control without *WKS1.1*. DMSO works as a negative control without an inhibitor. MG132 is a ubiquitin-mediated 26S proteasome inhibitor. E-64 is a cysteine protease inhibitor. Leu is a leupeptin, threonine, serine, and cysteine protease inhibitor. Peps (pepstatin A) is an aspartic peptidase inhibitor. NEMI is a cysteine protease inhibitor. Best (bestatin) is an arginine and alanine peptidase inhibitor. Apro (aprotitin) is a serine protease inhibitor.

Figure 6 A Predicted Working Model for PsbO in WKS1-Mediated *Pst* Resistance

After *Pst* infection, PsbO is bound and phosphorylated by WKS1.1 in thylakoids. Phosphorylated PsbO undergoes fast degradation by proteases, produces PsbO-free PSII, which has lower photosynthesis rate and works as a source for O_2^-, which is further converted to H_2O_2. H_2O_2 cannot be efficiently degraded by tAPX due to WKS1-mediated phosphorylation and accumulates to induce cell death, which inhibits *Pst* growth. H, haustoria. P, phosphorylation. tAPX, thylakoid ascorbate peroxidase.

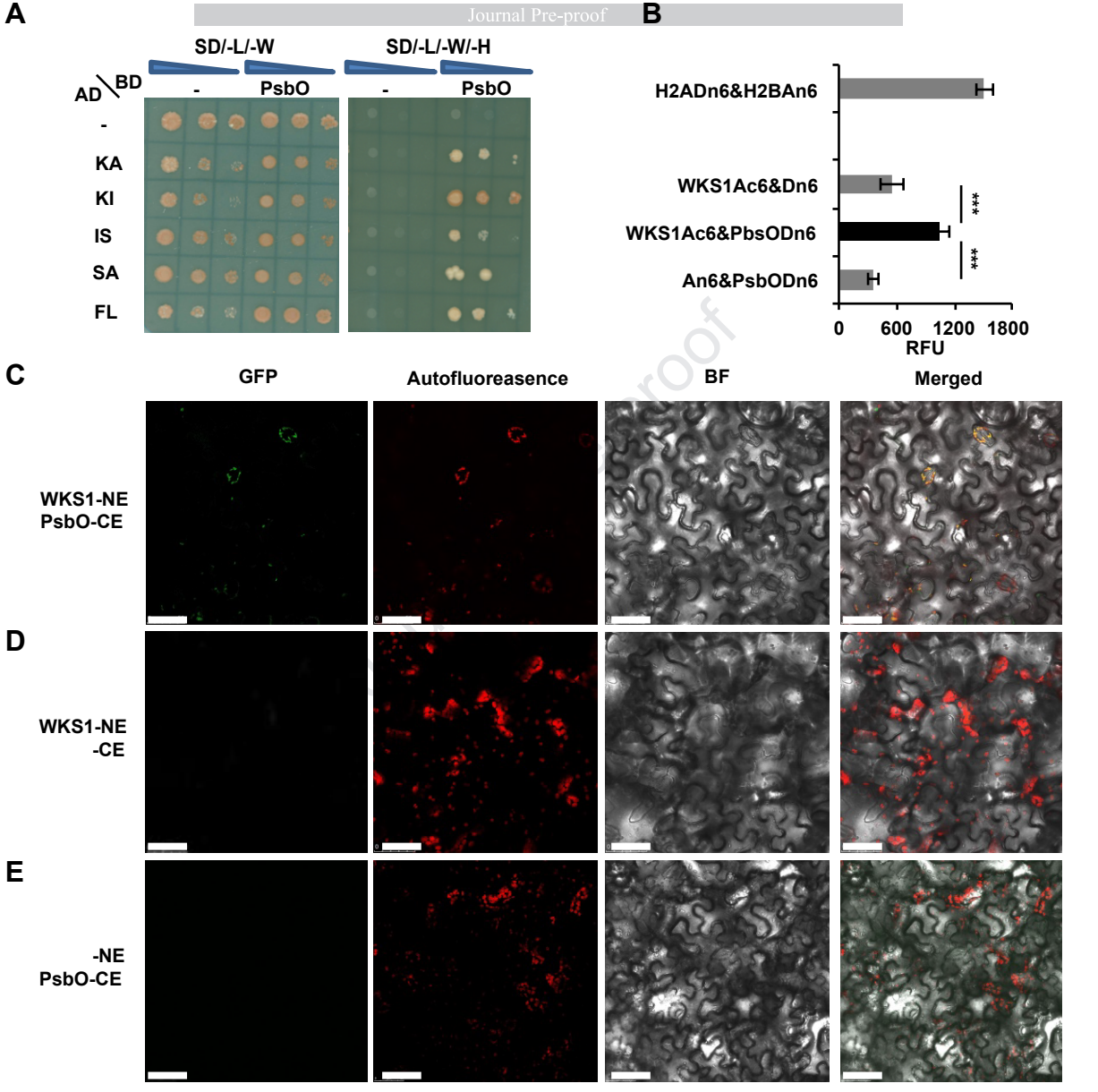

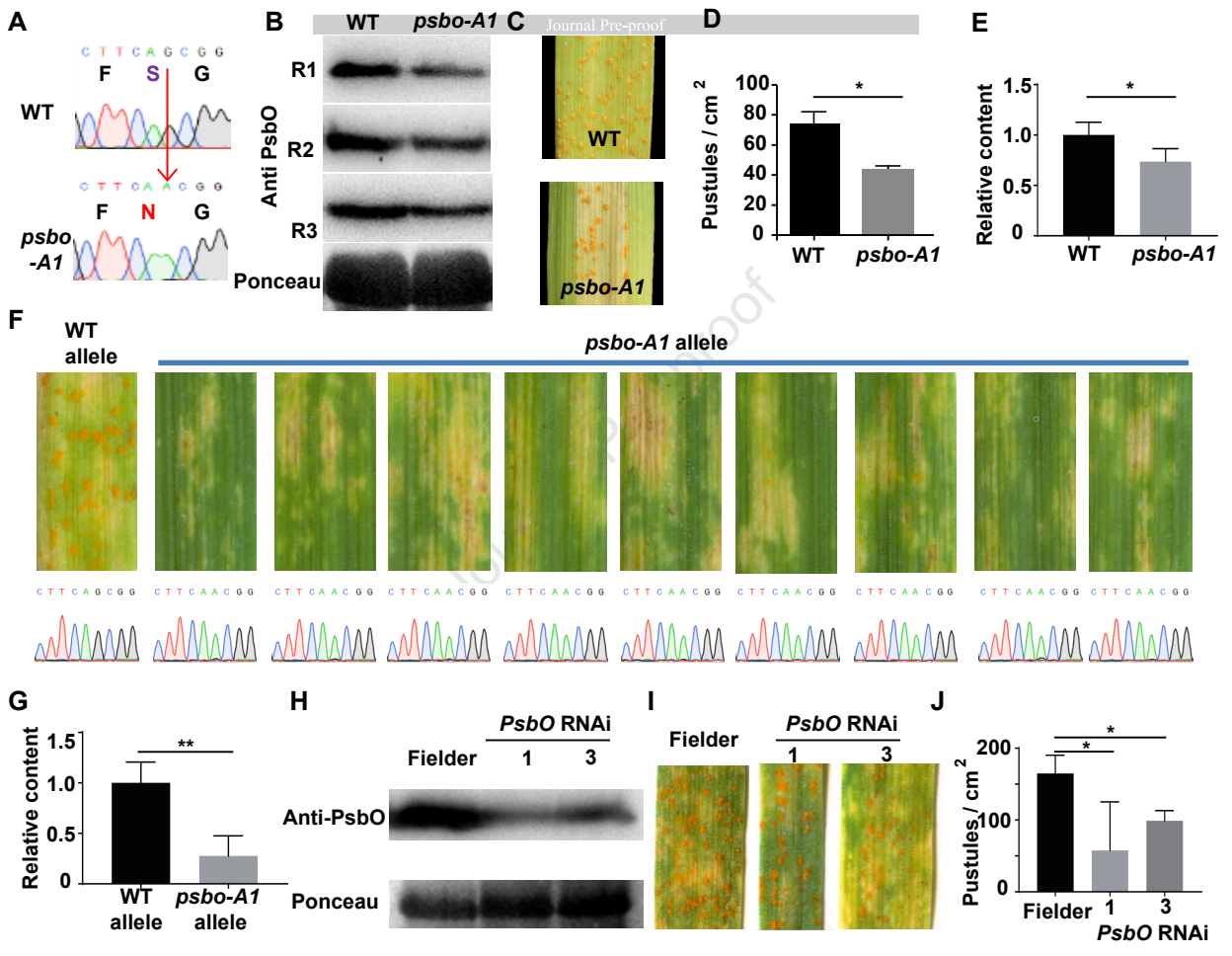
A
C T T C A G C G G
F S G
WT
C T T C A A C G G
F N G
psbo -A1
B
WT psbo-A1
R1
R2
R3
Anti PsbO
Ponceau
C
Journal Pre-proof
WT
psbo-A1
D
Pustules / cm 2
100
80
60
40
20
0
*
WT psbo-A1
E
Relative content
1.5
1.0
0.5
0
*
WT psbo-A1
F
WT allele
psbo-A1 allele
C T T C A G C G G
C T T C A A C G G
G
Relative content
1.5
1.0
0.5
0
**
WT allele
psbo-A1 allele
H
PsbO RNAi
Fielder 1 3
Anti-PsbO
Ponceau
I
Fielder
PsbO RNAi
1 3
J
Pustules / cm 2
200
100
0
*
*
Fielder 1 3
PsbO RNAi

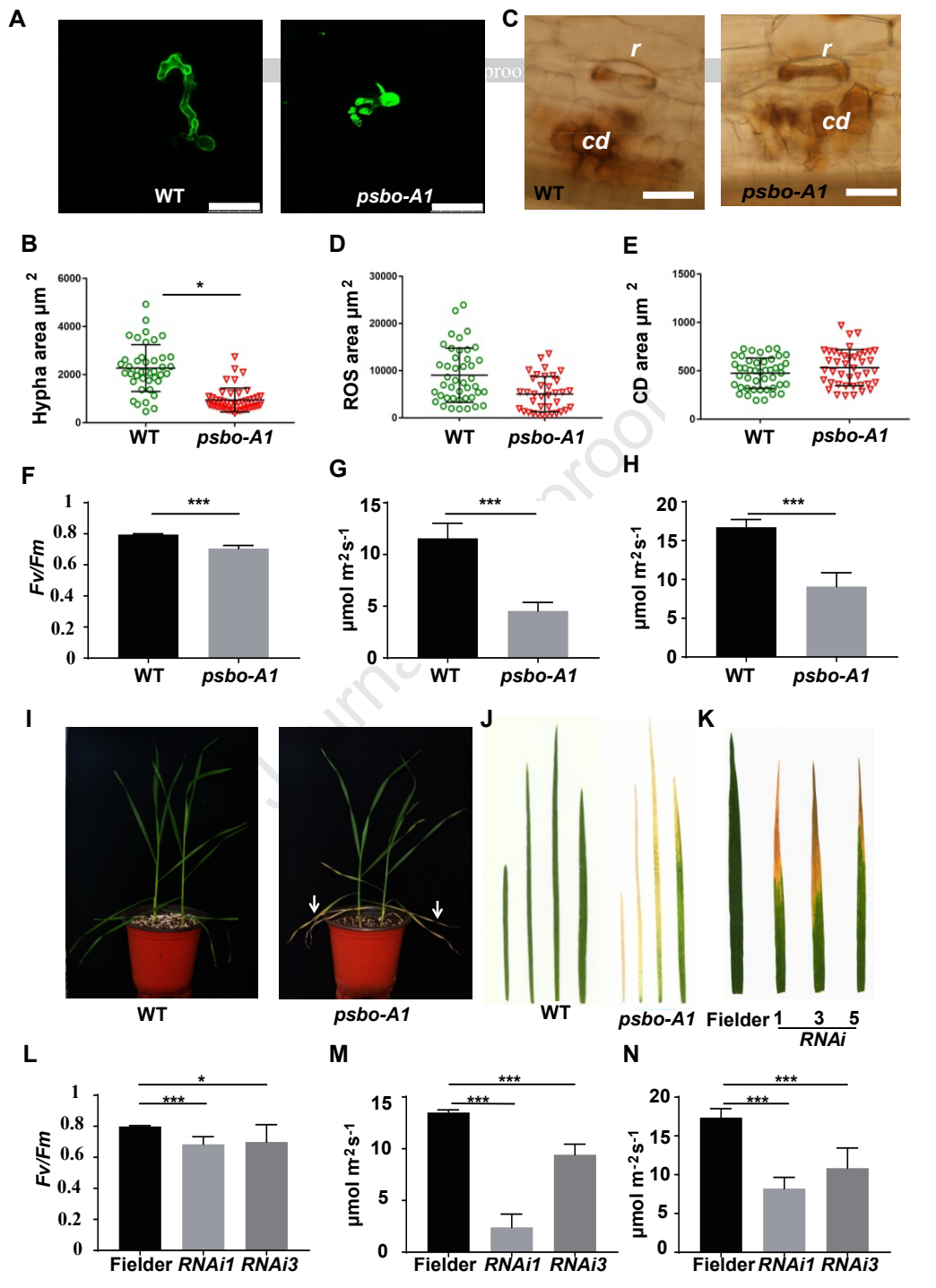
A
WT
psbo-A1
C
r
cd
WT
psbo-A1
B
Hypha area μm 2
WT
psbo-A1
D
ROS area μm 2
WT
psbo-A1
E
CD area μm 2
WT
psbo-A1
F
Fv/Fm
WT
psbo-A1
G
μmol m2s-1
WT
psbo-A1
H
μmol m2s-1
WT
psbo-A1
I
WT
psbo-A1
J
WT
psbo-A1
K
Fielder 1 3 5
RNAi
L
Fv/Fm
Fielder RNAi1 RNAi3
M
μmol m-2s-1
Fielder RNAi1 RNAi3
N
μmol m-2s-1
Fielder RNAi1 RNAi3

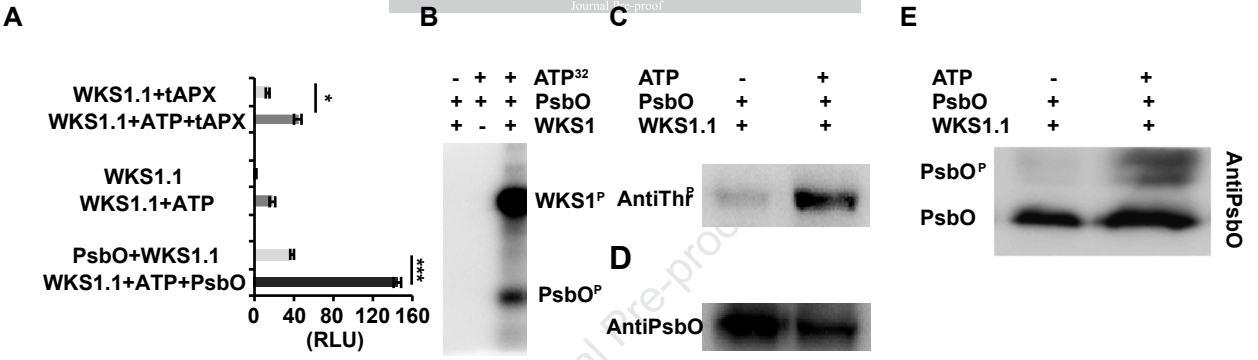

F

MAASLQAAATLMPAKIGGRASSARPSSHVARAFGVDAGTRITCS
LQSDIREVASKCADAAKMAGFALATSALLVSCASAEGAPKRLTF
DEIQSKTYMEVKGTGTANQCPTIDGGVDSFPFKAGKYEMKKF
CLEPTSFTVKAEGIQKNEPPAFQKTKLMTRLTYTLDEMEGPLEV
GADGTLKFEEkDGIDYAAVTVQLPGGERVPFLFTVKQLVATGKP
ESFSGPFLVPSYRGSSFLDPKGRGGSTGYDNAVALPAGGRGDE
EELAKENVKNASSSTGNITLSVTKSKPETGEVIGVFESVQPSDTD
LGAKAPkDVKIQGVWYAQLESN

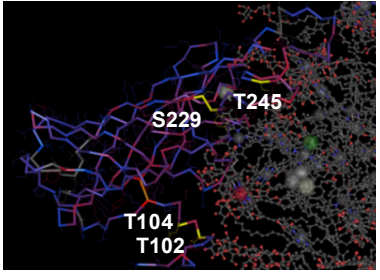

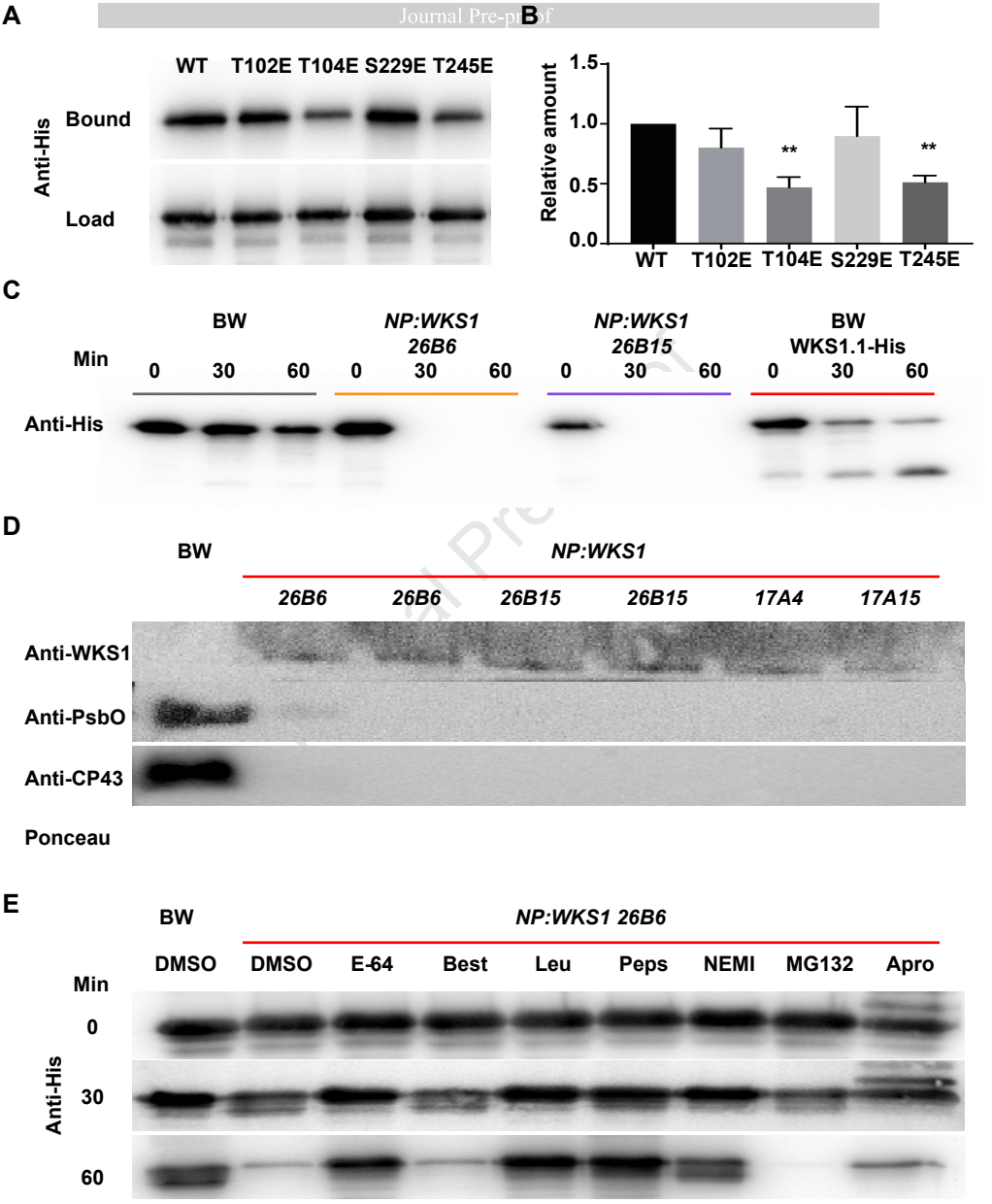

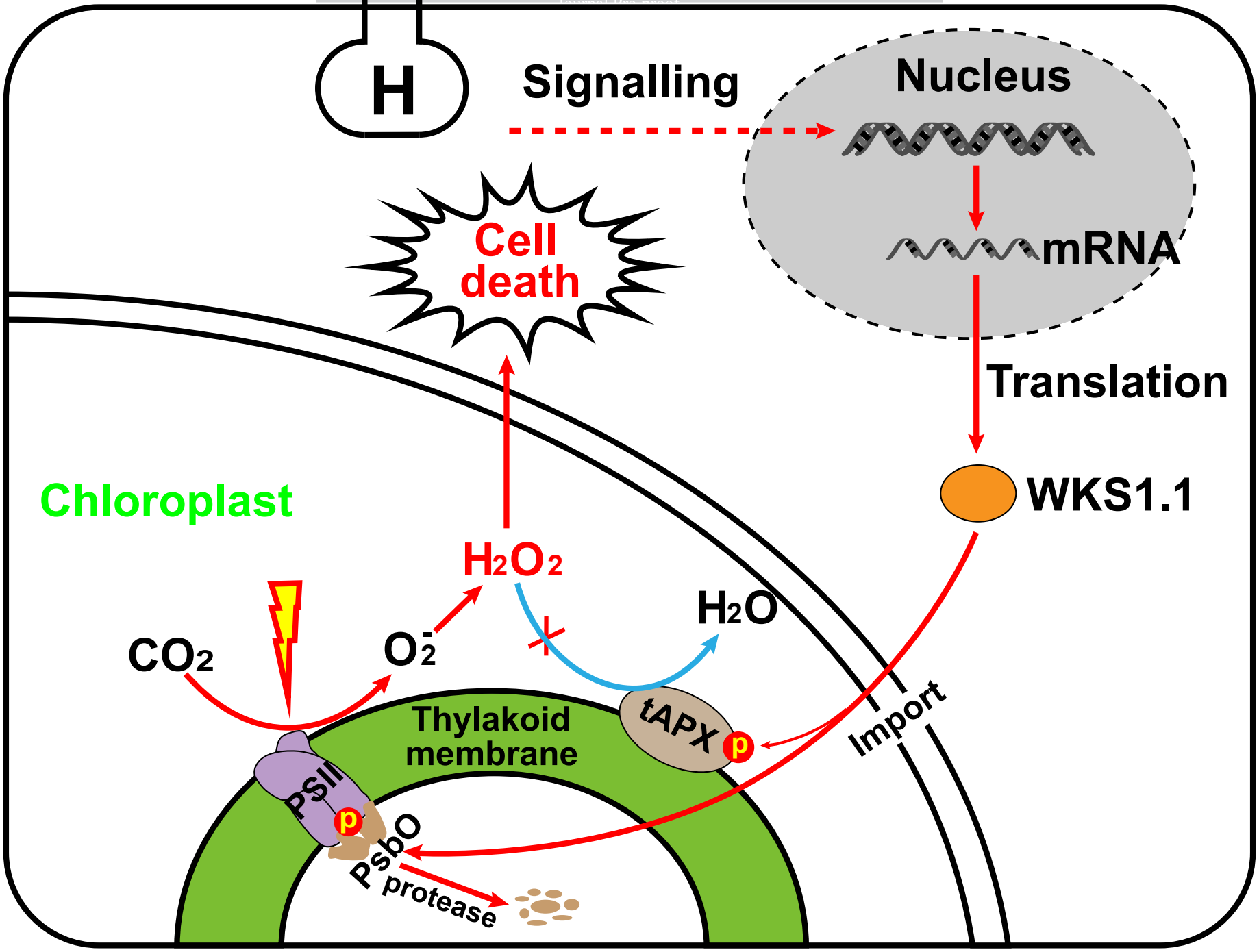
H
Signalling
Nucleus
mRNA
Cell death
Translation
Chloroplast
WKS1.1
H2O2
H2O
CO2
O2-
Thylakoid membrane
tAPX
p
Import
PSII
p
PsbO
protease